Atmospheric Boundary Layer at the coastal station, GMMC, well in comparison with the observed sounding at 0000 UTC.

Regarding the main factors leading to fog onset and dissipation, numerical results confirm all the findings of the observational analysis with more details about the interaction between the physical processes during the whole life cycle of the studied fog event. The onset stage was governed by weak turbulence and nocturnal radiative cooling at both stations while the mature phase and dissipation phase were slightly different. In fact, over the coastal station, GMMC, a zone of moisture flux convergence at the fog layer top, in addition to the coupling between the radiative cooling at the fog top and the vertical mixing, helped to maintain the fog layer. This coupling was also the main mechanism leading to the fog thickening at the inland station, GMMN. However, the dissipation phase at GMMN was governed by a zone of moisture divergence at the top of the fog layer, linked to the advection of dry air from the south, while a similar zone was located in the bottom of the fog layer over GMMC.

Sensitivity experiments to surface heterogeneities demonstrated that numerical coastal fog prediction was influenced by local topography and urbanization for this case study, but less by land cover. On the other hand, sensitivity experiments to aerosols pointed out that their impact was higher near the coast. It was found that the displacement of maritime aerosols over land had little impact on the fog patch at the inland station, while the continental aerosol potentially

433 influenced the life time of fog near the coast. In fact, continental droplets are smaller than the
434 maritime ones. This produces less gravitational settling and consequently higher liquid water
435 content.

436 This paper was limited to the study of an interesting case of advection-radiation fog in real
437 synoptic conditions in order to help to fill some gaps in our partial knowledge of the life cycle of
438 advection-radiation fog over heterogeneous coastal areas. Further investigation is needed with
439 emphasis on how fog forecasts can be improved over coastal regions, particularly over the Grand
440 Casablanca region in Morocco.

441

442 **REFERENCES**

443

444 Baars, J.A., Witiw, M., Al-Habash, A., Ramaprasad J. (2003). Determining fog type in the Los
445 Angeles basin using historic surface observation data. In Proc. 16th Conf. on Probability and
446 Statistics in the Atmospheric Sciences.

447 Bari, D., Bergot, T. and EL Khlifi, M. (2016). Local meteorological and large scale weather
448 characteristics of fog over the Grand Casablanca region, Morocco. *J. Appl. Meteor. Climatol*.
449 55(8): 1731-1745. doi: 10.1175/JAMC-D-15-03141.1.

450 Bari, D., Bergot, T. and EL Khlifi, M. (2015). Numerical study of a coastal fog event over
451 Casablanca, Morocco. *Q. J. R. Meteorolo. Soc.* 141: 1894-1905. doi:10.1002/qj.2494.

452 Bari, D. and EL Khlifi, M. (2015). LVP conditions at Mohamed V airport, Morocco: Local
453 characteristics and prediction using neural networks. *International Journal of Basic and*
454 *Applied Sciences*. 4(4): 354-363. doi: 10.14419/ijbas.v4i4.5044.
455 Bergot, T., Carrer, D., Noilhan, J. and Bougeault P. (2005). Improved Site-Specific Numerical
456 Prediction of Fog and Low Clouds: A Feasibility Study. *Wea. Forecasting*. 20: 627-646.
457 doi:10.1175/WAF873.1
458 Bergot, T., Terradellas, E., Cuxart, J., Mira, A., Liechti, O., Mueller, M., Nielsen, N.W. (2007).
459 Intercomparison of Single-Column Numerical Models for the Prediction of Radiation Fog. *J.*
460 *Appl. Meteor. Clim.* 46:504-521.
461 Bergot, T. (2013). Small-scale structure of radiation fog: a large-eddy simulation study. *Q. J. R.*
462 *Meteorol. Soc.* 139: 1099-1112.
463 Bergot, T., Escobar, J. and Masson V. (2014). Effect of small scale surface heterogeneities and
464 buildings on radiation fog : Large-Eddy Simulation study at Paris-Charles de Gaulle airport. *Q.*
465 *J. R. Meteorol. Soc.* doi: 10.1002/qj.2358.
466 Bougeault, P. and Lacarrère, P. (1989). Parameterization of orography-induced turbulence in a
467 mesobeta-scale model. *Mon. Wea. Rev*. 117:1872-1890.
468 Boutle, I.A., Finnenkoetter, A., Lock, A.P. and Wells, H. (2016), The London Model: forecasting
469 fog at 333 m resolution. *Q. J. R. Meteorol. Soc.,* 142: 360–371. doi:10.1002/qj.2656

Cermak, J., Bendix, J. (2007). Dynamical Nighttime Fog/Low Stratus Detection Based on Meteosat SEVIRI Data: A Feasibility Study. Pure Appl. Geophys. 164: 1179-1192.

Charnock, H. (1955). Wind stress on a water surface. *Q. J. R. Meteorol. Soc.* 81: 639-640

Cohard, J.-M., Pinty, J.-P. and Suhre, K. (2000). On the parameterization of activation spectra from cloud condensation nuclei microphysical properties. *Journal of Geophysical Research*. 105 (D9), 11753–11766.

Cuxart, J., Bougeault, P. and Redelsperger, J.L. (2000). A turbulence scheme allowing for mesoscale and large-eddy simulations. *Q. J. R. Meteorol. Soc*. 126: 1-30.

Cuxart, J. and Jiménez, M.A. (2007). Mixing processes in a nocturnal low-level jet: An LES study. *Journal of the atmospheric sciences*. 64(5): 1666-1679.

Cuxart, J. and Jiménez, M.A. (2012). Deep radiation fog in a wide closed valley: Study by numerical modeling and remote sensing. *Pure. Appl. Geophys*. 169:911-926.

Dee, D.P., Uppala, S.M., Simmons, A.J., Berrisford, P., Poli, P., Kobayashi, S., Andrae, U., Balmaseda, M.A., Balsamo, G., Bauer, P., Bechtold, P., Beljaars, A.C.M, van de Berg, L., Bidlot, J., Bormann, N., Delsol, C., Dragani, R., Fuentes, M., Geer, A.J., Haimberger, L., Healy, S.B., Hersbach, H., Hólm, E.V., Isaksen, L., Källberg, P., Köhler, M., Matricardi, M., McNally, A.P., Monge-Sanz, B.M., Morcrette, J.J., Park, B.K., Peubey, C., de Rosnay, P., Tavolato, C., Thépaut, J.N., Vitart, F. (2011). The ERA-Interim reanalysis: configuration and

performance of the data assimilation system. *Q. J. R. Meteorol. Soc*. 137: 553-597.

Durran, D.R. (1989). Improving the anelastic approximation. *Journal of the atmospheric sciences*. 46(11): 1453-1461.

Duynkerke, P.G. (1991). Radiation fog: A comparison of model simulation with detailed observations. *Monthly Weather Review*. 119(2): 324-341.

Dupont, J.C., Haeffelin, M., Protat, A., Bouniol, D., Boyouk, N. and Morille, Y. (2012). Stratus fog formation and dissipation: a 6-day case study. *Boundary-layer meteorology*. 143(1): 207-225.

George, J.J. (1951). Fog. Compendium of meteorology, 1179-1189.

Gheusi, F., Stein, J. (2002). Lagrangian description of airflows using Eulerian passive tracers. *Quarterly Journal of the Royal Meteorological Society*. 128(579): 337-360.

Gultepe, I., Tardif, R., Michaelides, S.C., Cermak, J., Bott, A., Bendix, J., Müller, M.D., Pagowski, M., Hansen, B., Ellrod, G., Jacobs, W., Toth, G. and Cobe, S.G. (2007). Fog Research: A Review of Past Achievements and Future Perspectives. *Pure Appl. Geophys*. 164: 1121-1159.

Hilliker, J.L. and Fritsch, J.M. (1999). An observations-based statistical system for warm-season hourly probabilistic forecasts of low ceiling at the San Francisco International Airport. *Journal of Applied Meteorology*. 38(12): 1692-1705.

506 Khairoutdinov, M., and Kogan, Y. (2000). A new cloud physics parameterization in a large-eddy
507 simulation model of marine stratocumulus. *Monthly Weather Review.* 128 (1), 229–243.
508 Koracin, D., Lewis, J., Thompson, W.T., Dorman, C.E. and Businger, J.A. (2001). Transition of
509 stratus into fog along the California Coast: Observations and modeling. *J. Atmos. Sci.* 58:
510 1714-173
511 Lafore, J.P., Stein, J., Asencio, N., Bougeault, P., Ducrocq, V., Duron, J., Fischer, C., Hereil, P.,
512 Mascart, P., Pinty, J.P., Redelsperger, J.L., Richard, E., De Arellano, J.V.G. (1998). The Meso-
513 NH Atmospheric Simulation System. Part I: Adiabatic formulation and control simulations.
514 *Ann. Geophys*. 16: 90-109.
515 Martínez, D., Jiménez, M. A., Cuxart, J. and Mahrt, L. (2010). Heterogeneous nocturnal cooling
516 in a large basin under very stable conditions. *Boundary-layer meteorology*. 137(1): 97-113.
517 Musson-Genon, L. (1987). Numerical simulation of a fog event with a one-dimensional boundary
518 layer model. *Monthly Weather Review*. 115(2): 592-607.
519 Masson V. (2000). A physically based scheme for the urban energy budget in atmospheric
520 models. *Bound.-Lay. Meteorol*. 94: 357-397.
521 Masson, V., Champeaux, J.L., Chauvin, F., Meriguet, C. and Lacaze, R. (2003). A global
522 database of land surface parameters at 1-km resolution in meteorological and climate models.
523 *Journal of climate*. 16(9): 1261-1282.

524 Mironov, D., Golosov, S., Heise, E., Kourzeneva, E., Ritter, B., Scheider, N. and Terzhevik, A.
525 (2005). Flake - A Lake Model for Environmental Applications. In Proceedings of the 9th
526 Workshop on Physical Processes in Natural Waters, Lancaster University, UK, September
527 2005, A. Folkard and I. Jones, Eds.
528 Mlawer, E.J., Taubman, S.J., Brown, P.D., Iacono, M.J., Clough, S.A. (1997). Radiative transfer
529 for inhomogeneous atmospheres: RRTM, a validation correlated-k model for the longwave. *J.*
530 *Geophys. Res.* 102:16663-16682.
531 Morcrette, J.J. (1991). Radiation and cloud radiative properties in the European Centre for
532 Medium Range Weather Forecasts forecasting system. *J. Geophys. Res*. 96: 9121-9132.
533 Niu, S., Lu, C., Yu, H., Zhao, L. and Lü, J. (2010). Fog research in China: an overview. *Adv.*
534 *Atmos. Sci.* 27: 639-662.
535 Noilhan, J., Mahfouf, J.F. (1996). The ISBA land surface parameterization scheme. *Global*
536 *Planet. Change.* 13: 145-159.
537 Petterssen, S. (1939). Some aspects of formation and dissipation of fog. *Geofys. Publ.* 12, 522.
538 Philip, A., Bergot, T., Bouteloup, Y. and Bouyssel, F. (2016). The Impact of Vertical Resolution
539 on Fog Forecasting in the Kilometric-Scale Model AROME: A Case Study and Statistics. *Wea.*
540 *Forecasting*. 31: 1655-1671. DOI: 10.1175/WAF-D-16-0074.1.
541 Pinty, J.P. and Jabouille, P. (1998). A mixed-phase cloud parameterization for use in mesoscale

non-hydrostatic model: simulations of a squall line and of orographic precipitations. In Proceedings Conf. of Cloud Physics, Everett, WA, USA, Amer. Meteor. Soc.

Press, W.H., Teukolsky, S.A., Vetterling, W.T. and Flannery, B.P. (1992). Numerical Recipes in FORTRAN: The Art of Scientific Computing. 2nd ed., 963 pp, Univ. Press, Cambridge, New York.

Ryznar, E. (1977). Advection-radiation fog near Lake Michigan. *Atmospheric Environment*. 11(5): 427-430.

Roquelaure, S., Tardif, R., Remy, S. and Bergot T. (2009). Skill of a Ceiling and Visibility Local Ensemble Prediction System (LEPS) according to Fog-Type Prediction at Paris-Charles de Gaulle Airport. *Wea. Forecasting*. 24: 15111523. doi: 10.1175/2009WAF2222213.1

Román-Cascón, C., Steeneveld, G. J., Yagüe, C., Sastre, M., Arrillaga, J. A. and Maqueda, G. (2016). Forecasting radiation fog at climatologically contrasting sites: evaluation of statistical methods and WRF. *Q. J. R. Meteorol. Soc*. 142: 1048–1063. doi:10.1002/qj.2708

Sandu, I., Brenguier, J.L., Geoffroy, O., Thouron, O., Masson, V. (2008). Aerosol impacts on the diurnal cycle of marine stratocumulus. *J. Atmos. Sci.* 65: 27052718.

Tardif, R. (2007). The impact of vertical resolution in the explicit numerical forecasting of radiation Fog: A Case Study. *Pure Appl. Geophys*. 164: 1221-1240.

Tardif, R., and Rasmussen, R.M. (2007). Event-based climatology and typology of fog in the

New York City region. *J. Appl. Meteor. Clim*. 46:1141-1168.

Tardif, R., and Rasmussen, R. M. (2008). Process-oriented analysis of environmental conditions associated with precipitation fog events in the New York City region. *Journal of Applied Meteorology and Climatology*, 47(6), 1681-1703.

Taylor, G.I. (1917). The formation of fog and mist. *Q. J. R. Meteorol. Soc*., 43: 241268. doi: 10.1002/qj.49704318302

Ye, X., Wu, B. and Zhang, H. (2015). The turbulent structure and transport in fog layers observed over the Tianjin area. *Atmospheric Research*. 153: 217-234.

WMO. (1992). International meteorological vocabulary. WMO Publication 182. World Meteorological Organization: Geneva, Switzerland

571

572 **Table 1.** Summary of the setup of the run

Features	Details
Domains	2, one-way nested
Outer domain	500 km x 500 km (100x100 grid points)
Inner domain	100 km x 100 km (100x100 grid points)
Horizontal Resolution	5 km (outer domain), 1 km (inner domain)
Vertical resolution	60 levels, first level at 2m, 4 levels below 10m, 18 levels below 100m and 39 levels in the lowest 1000m
Time step	15s (outer domain), 5s (inner domain)
Equation system	Non-hydrostatic primitive equation of Durran (1989)
Lateral boundary conditions	Analysis from the ECMWF every 6 hours (Dee et al. (2011))
Microphysics scheme	1-moment mixed scheme (Pinty and Jabouille (1998))
	Sedimentation of droplets is allowed (Bergot et al. (2007))
Radiation scheme	Long-wave radiation Mlawer et al. (1997)
	Short-wave radiation Morcrette (1991)
Turbulence Scheme	1-Dimensional TKE scheme Cuxart et al. (2000)
	Mixing length Bougeault and Lacarrère (1989)
Soil Scheme	Interaction between Soil, Biosphere and Atmopshere (Noilhan and Mahfouf (1996))
	Fluxes over marine surfaces Charnock (1955)
	Urban and artificial areas Masson (2000)
Surface features	Land cover : ECOCLIMAP, global map, 1km resolution, Masson et al. (2003)
	Orography: GTOPO30, global map, 1km resolution
	Sand and clay fractions : FAO, 1988, global map, 10km resolution

573

574 **Table 2.** Summary of the sensitivity experiments

Experiments	Microphysical Parameterization	Details
KHKOC	Two-moment	Continental aerosols
KHKOM	Two-moment	Maritime aerosols
NORELIEF	Single-moment	The orography is removed
BARESOIL	Single-moment	Land cover is supposed uniform bare soil
URBAN	Single-moment	Land cover is supposed uniform urban where buildings fraction is 30%, and building height is 10 m

575

576 **Table 3.** Onset and dissipation times from the control and sensitivity experiments.
577 Uncertainty in hours between each sensitivity experiment and the control one is shown in
578 parentheses.

Experiments	The coastal station GMMC		The inland station GMMC	
	Onset	Dissipation	Onset	Dissipation
REFEXP	2100UTC	0300UTC	2000UTC	0200UTC
NORELIEF	2200UTC (+1h)	After 0600UTC	2000 UTC (+0h)	After 0600 UTC
BARESOIL	2000UTC (-1h)	0200UTC (-1h)	2100 UTC (+1h)	0000 UTC (-2h)
URBAN	0000UTC (+3h)	0400UTC (+1h)	0000 UTC (+4h)	0200 UTC (+0h)
KHKOM	1900UTC (-2h)	0200UTC (-1h)	2000 UTC (+0h)	0000 UTC (-2h)
KHKOC	1900UTC (-2h)	0300UTC (+0h)	2000 UTC (+0h)	0000 UTC (-2h)

579

Figure Captions

Fig. 1. (a) Map showing the land cover of the GCB region, with the locations of the two synoptic stations used in this study, (b) Map showing the topographical (m) and physiographic features of the region of interest.

Fig. 2. Mean sea level pressure spatial distribution at (a) 1200UTC on 23 December, (b) at 1800UTC on 23 December, and (c) at 0600UTC on 24 December. The gray square refers to the GCB region. The empty square refers to a domain that will be used in the numerical simulation.

Fig. 3. Time series of conventional meteorological parameters: (top to bottom) cloud height base (m a.g.l), horizontal visibility (km), 10m wind direction (1/10°), 10m wind speed (m s^{-1}) and 2m temperature (°C), for GMMC (dashed line) and GMMN (solid line) over the period from 0000UTC on 23 December to 1200UTC on 24 December. The vertical bars refer to the observed onset and dissipation times of the fog event at GMMC (dashed line) and GMMN (solid line). The horizontal lines in the visibility plot refer to the fog (1km, long-dashed line) and mist (5km, dot-dashed line) thresholds. Sunrise and sunset times are shown.

Fig. 4. MSG derived image, following Cermak and Bendix's (2007) approach, during: (a) the formation (2100UTC on 23 Dec 2013), (b) the mature (0000UTC on 24 Dec 2013) and (c) the dissipation (0600UTC on 24 Dec 2013) phases. Square refers to MNH1.

Fig. 5. The liquid water path in the lowest kilometer (1-km LWP) from MNH5 (left) and MNH1 (middle), and liquid water content at 2m from MNH1 (right) during: formation phase (2100UTC, top row) and dissipation phase (0600UTC, bottom row). Filled triangle and square refer to GMMN and GMMC respectively. Square in MNH5 refers to MNH1.

Fig. 6. (a) Time series of the 1-km resolution model simulated 2-m temperature (°C), wind speed (m s^{-1}), wind direction (°), and 2-m relative humidity (%) at the coastal station GMMC (circles, dashed line) and at the inland station GMMN (triangles, solid line). Simulated SST (stars) is superimposed on temperatures plot. The period covers from 1200 UTC on 23 December to 0600 UTC on 24 December. The vertical bars refer to the onset and dissipation times of the simulated fog event at GMMC (dashed line) and GMMN (solid line). (b) Simulated sounding superimposed on observed sounding at 0000 UTC on 24 December 2013 at the coastal station GMMC: temperature (circle for observation and solid line with x for simulation) and dew-point temperature (+ for observation and dashed line with * for simulation).

Fig. 7. (a) The 9 h back trajectories of air parcels ending at GMMC and GMMN, on 23 December 2013 at 2100 UTC, at the heights above ground level of 2 m (solid line), 10 m (dashed line) and 50 m (dotted line). (b) Time series of simulated water vapor mixing ratio (g kg^{-1}), air temperature (°C) superimposed on dew point temperature (°C) and height (m a.s.l) along the back-trajectory with ending point at 2 m at GMMC (solid line with star) located at 60 m a.s.l and GMMN (dashed line with circle) located at 200 m a.s.l on 23 December at 2100 UTC. The vertical line corresponds to the time when the parcel reached the continental part of the coastal region (dashed line for GMMN and solid line for GMMC).

Fig. 8. Time-height contour plots of (a) and (d) simulated horizontal moisture flux divergence (10^{-5} g kg^{-1} s^{-1}), (b) and (e) simulated radiative cooling (10^{-3} K s^{-1}) and (c) and (f) turbulent kinetic energy (m^2 s^{-2}) at inland station GMMN (top) and coastal station GMMC (bottom).

Fig. 9. Time-height contour plots of simulated LWC (g kg^{-1}), from REFEXP and sensitivity experiments (NORELIEF, BARESOIL, URBAN, KHKOM and KHKOC) at the inland station GMMN.

Fig. 10. Time-height contour plots of simulated LWC (g kg^{-1}), from REFEXP and sensitivity experiments (NORELIEF, BARESOIL, URBAN, KHKOM and KHKOC) at the coastal station GMMC.

Fig. 11. The simulated 10 m wind superimposed on liquid water content at 2 m (g kg^{-1}) from MNH5 during the mature phase (24 Dec 2013 at 0000 UTC), issued from REFEXP and sensitivity experiments (NORELIEF, BARESOIL, URBAN, KHKOM and KHKOC). Filled triangle and square indicate locations of GMMN and GMMC, respectively. Square refers to MNH1.

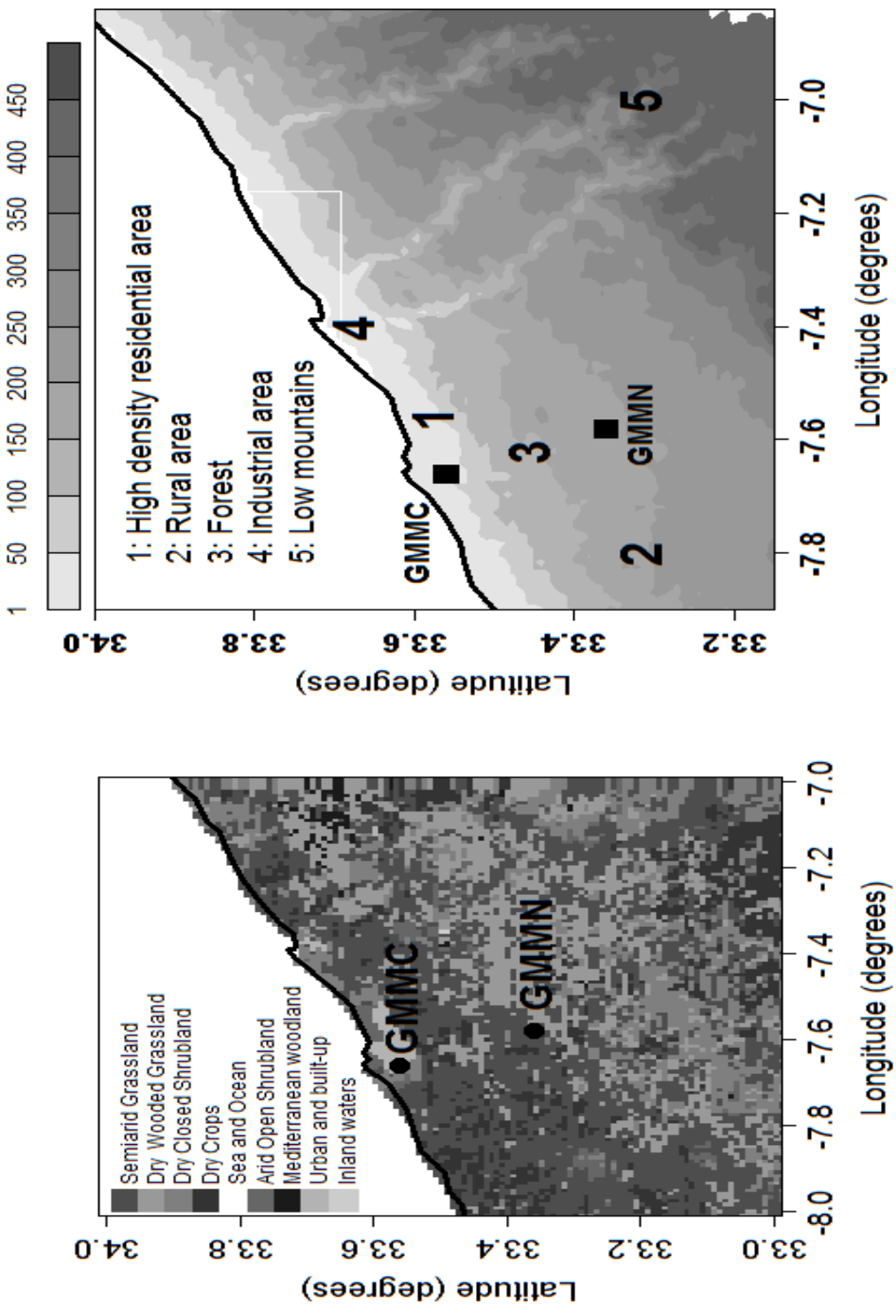

645

646 **Fig. 1.**

647

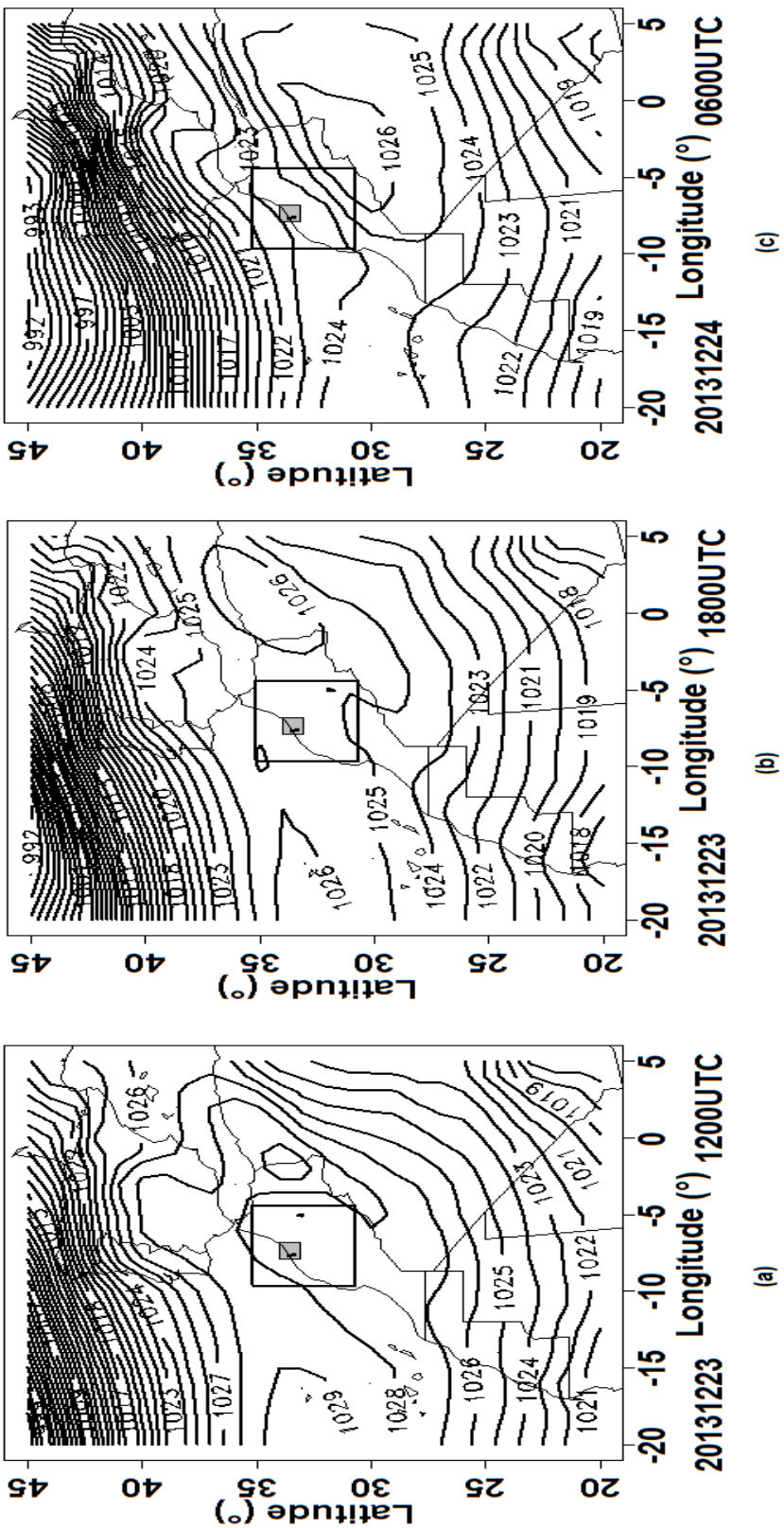
20131223 1200UTC
20131223 1800UTC
20131224 0600UTC
Longitude (°)
Latitude (°)
(a)
(b)
(c)

Fig. 2.

650

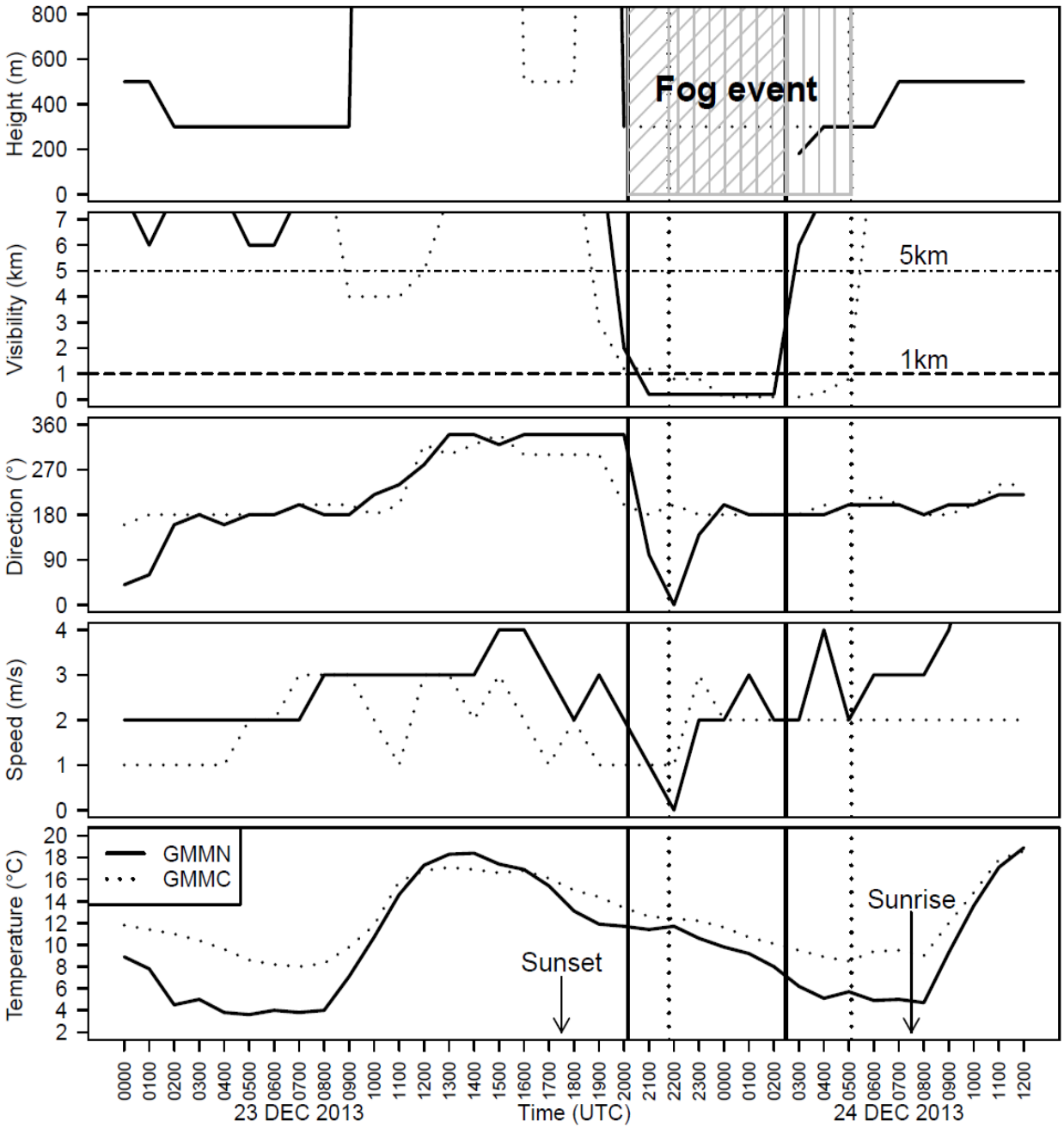

651

652

653 **Fig. 3.**

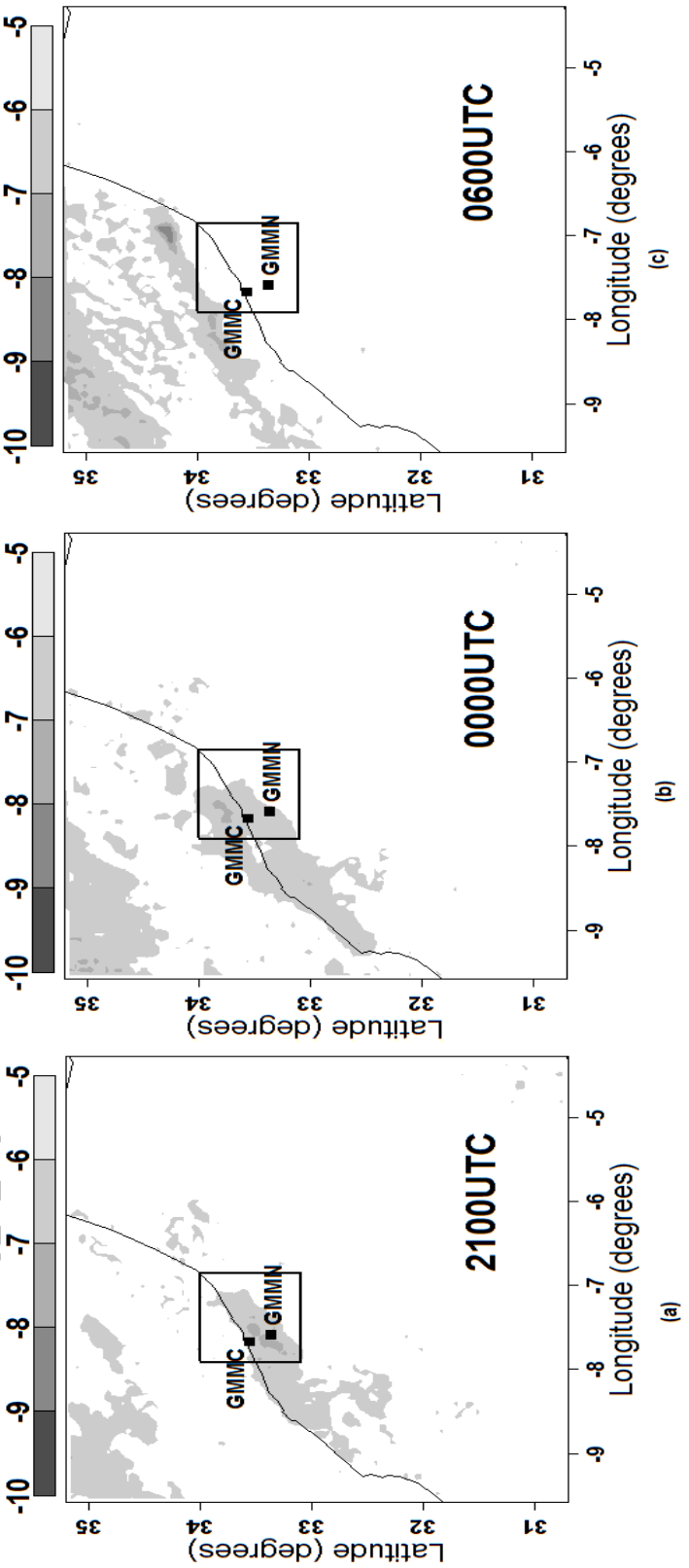

654

655 **Fig. 4.**

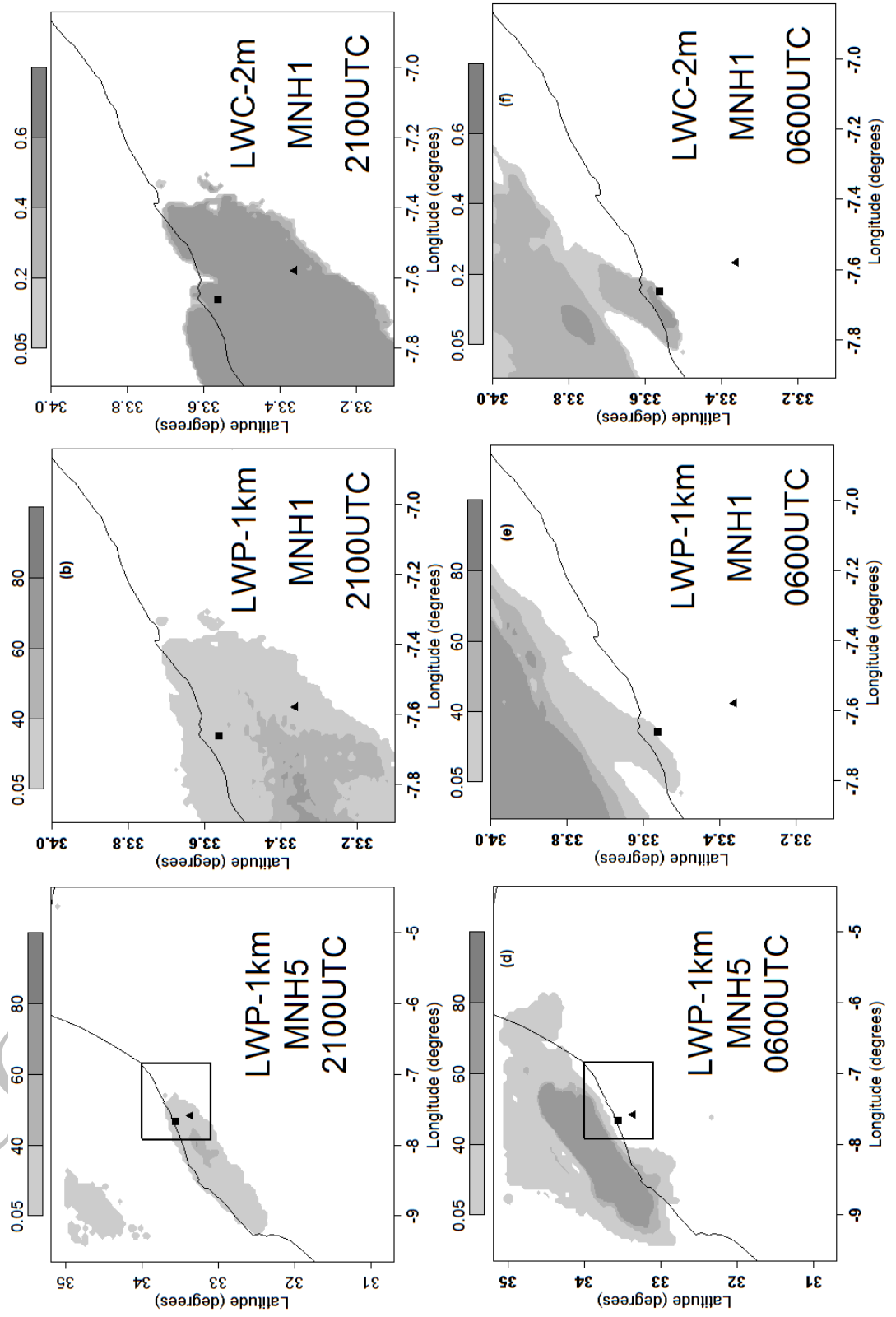
LWP-1km
MNH5
2100UTC
LWP-1km
MNH1
2100UTC
LWC-2m
MNH1
2100UTC
LWP-1km
MNH5
0600UTC
LWP-1km
MNH1
0600UTC
LWC-2m
MNH1
0600UTC
(b)
(d)
(e)
(f)
Latitude (degrees)
Longitude (degrees)

Fig. 5.

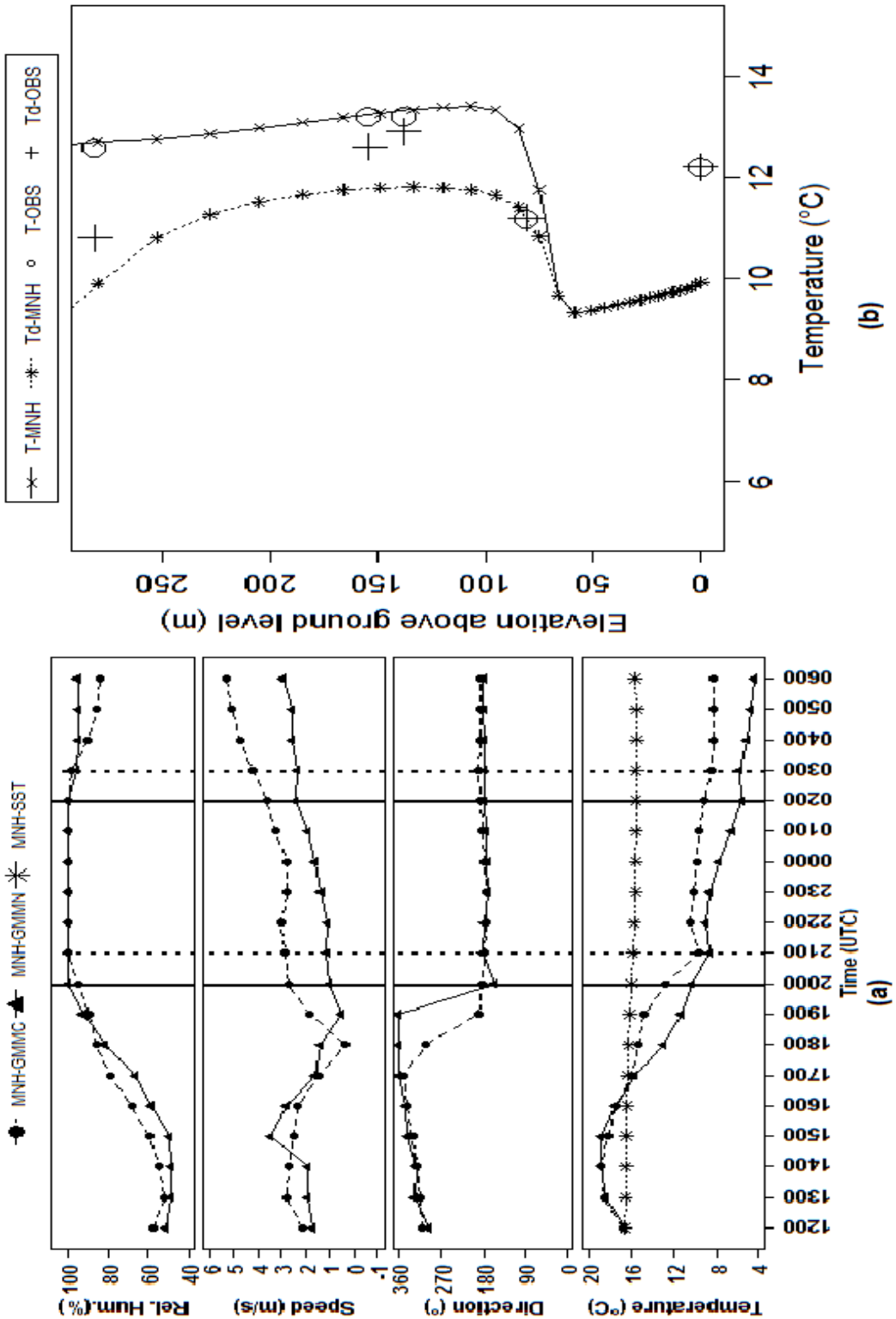
MNH-GMMC
MNH-GMMN
MNH-SST
Rel. Hum.(%)
Speed (m/s)
Direction (°)
Temperature (°C)
Time (UTC)
(a)
T-MNH
Td-MNH
T-OBS
Td-OBS
Elevation above ground level (m)
Temperature (°C)
(b)

Fig. 6.

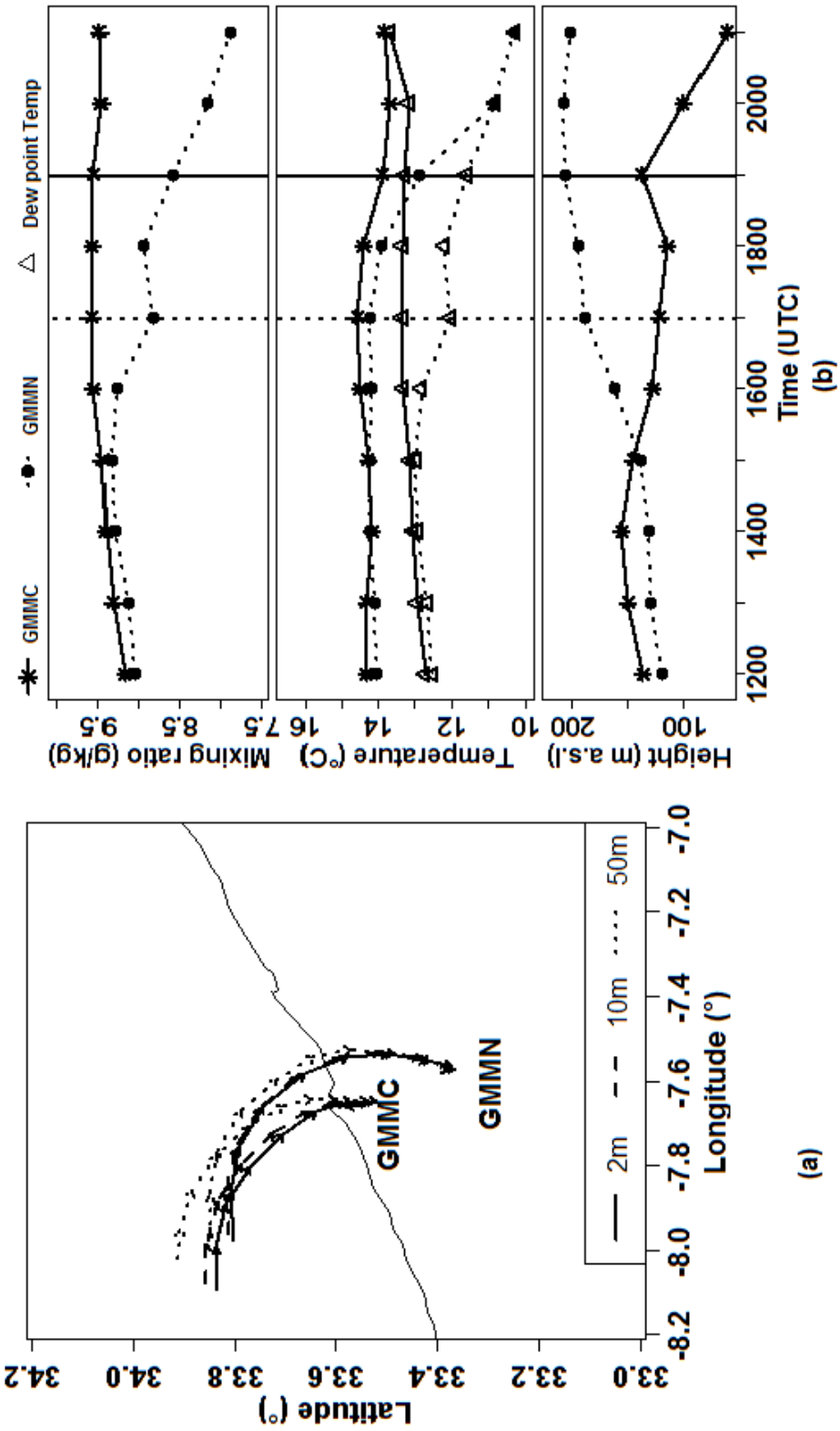

661

662 **Fig. 7.**

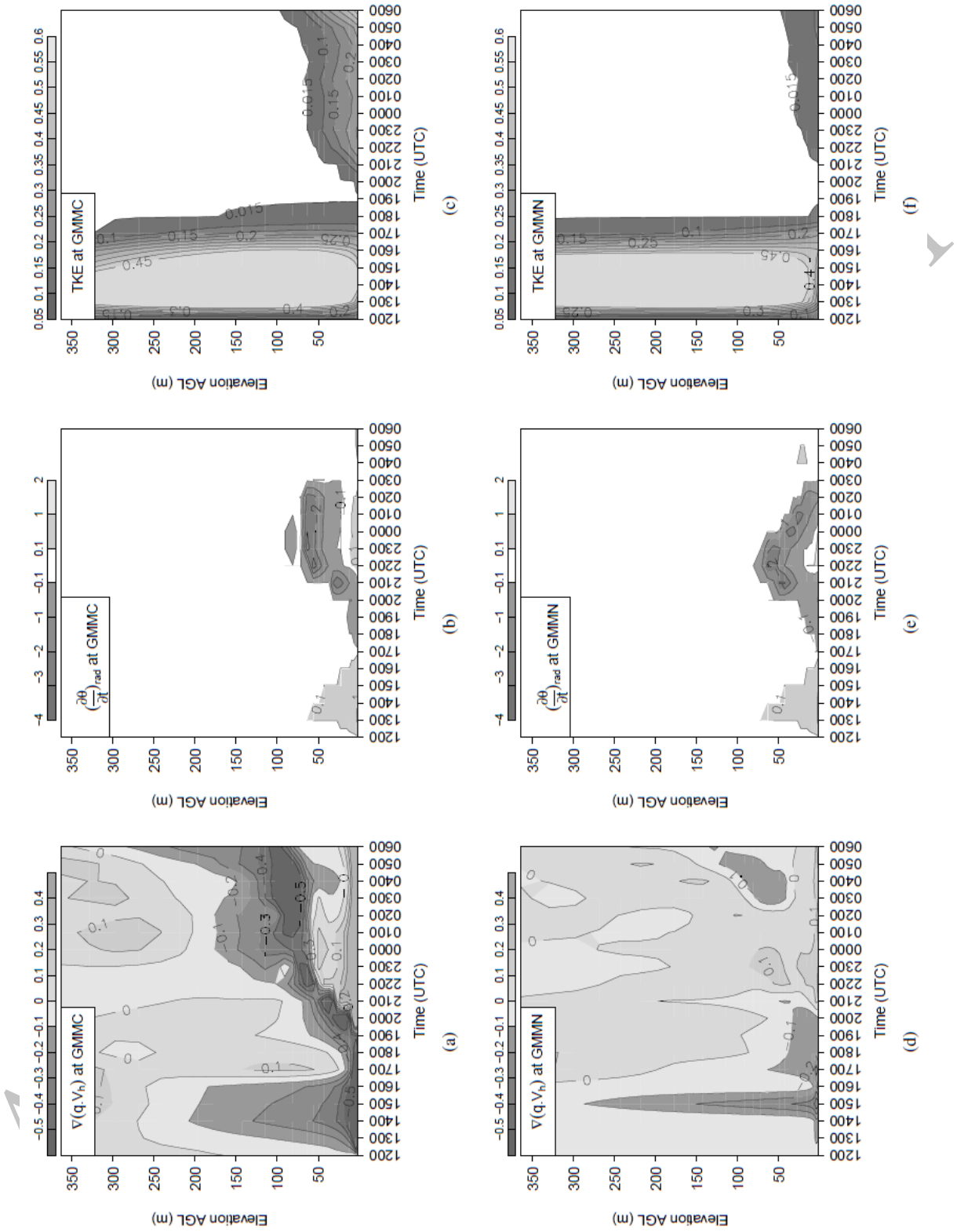

663

664 **Fig. 8.**

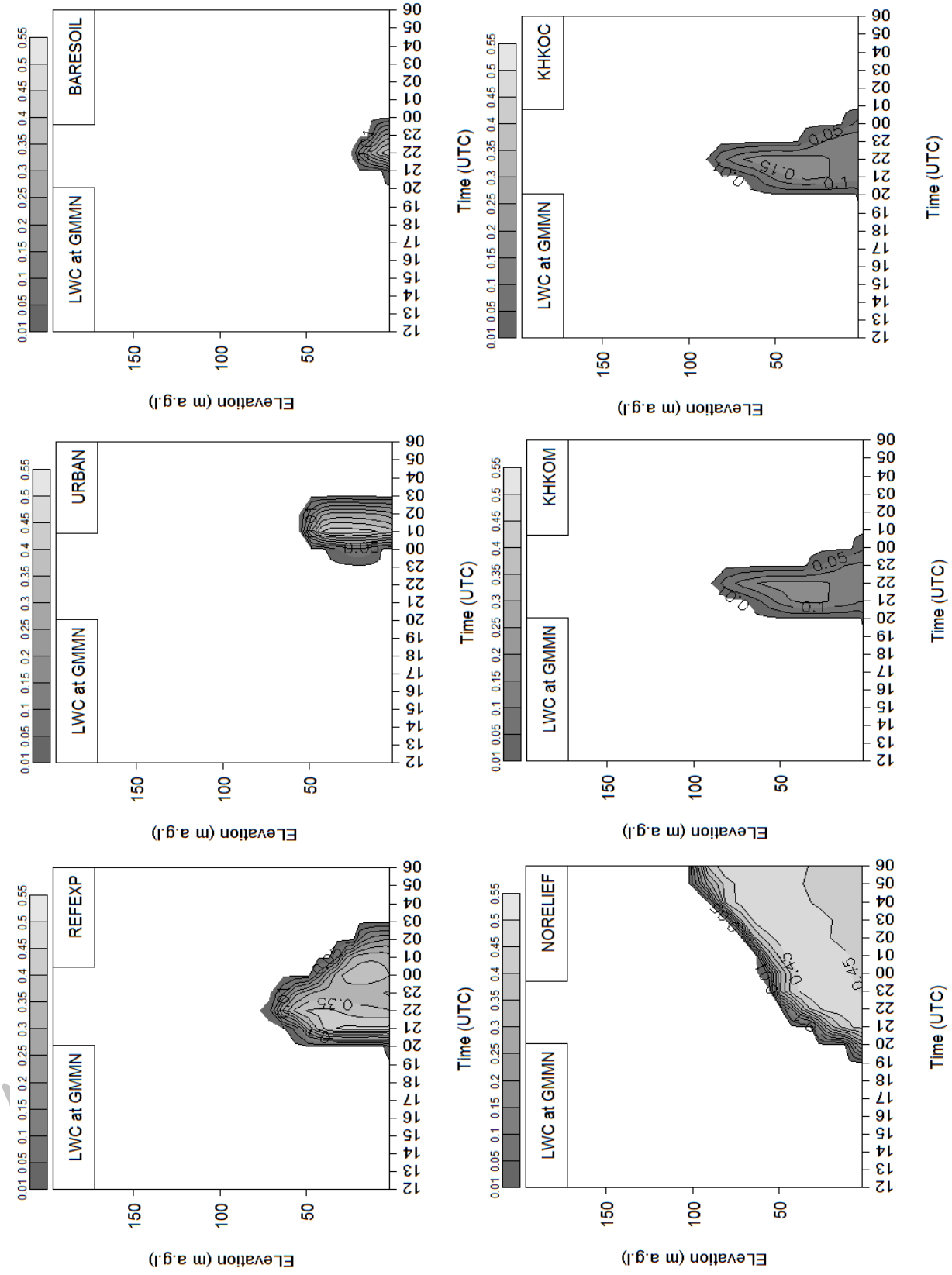
LWC at GMMN
REFEXP
URBAN
BARESOIL
NORELIEF
KHKOM
KHKOC
Time (UTC)
Elevation (m a.g.l)

665

666 **Fig. 9.**

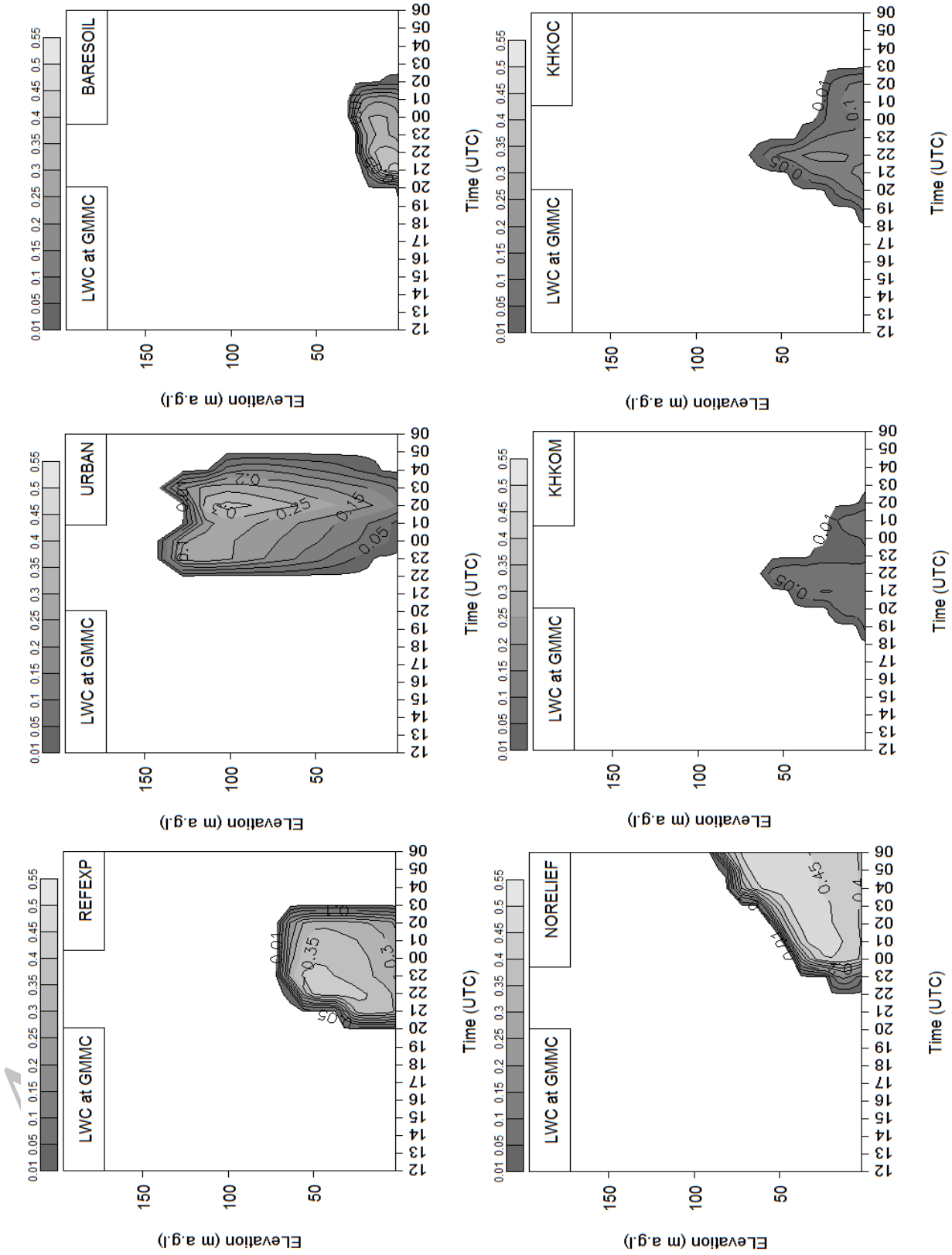

667

668 **Fig. 10.**

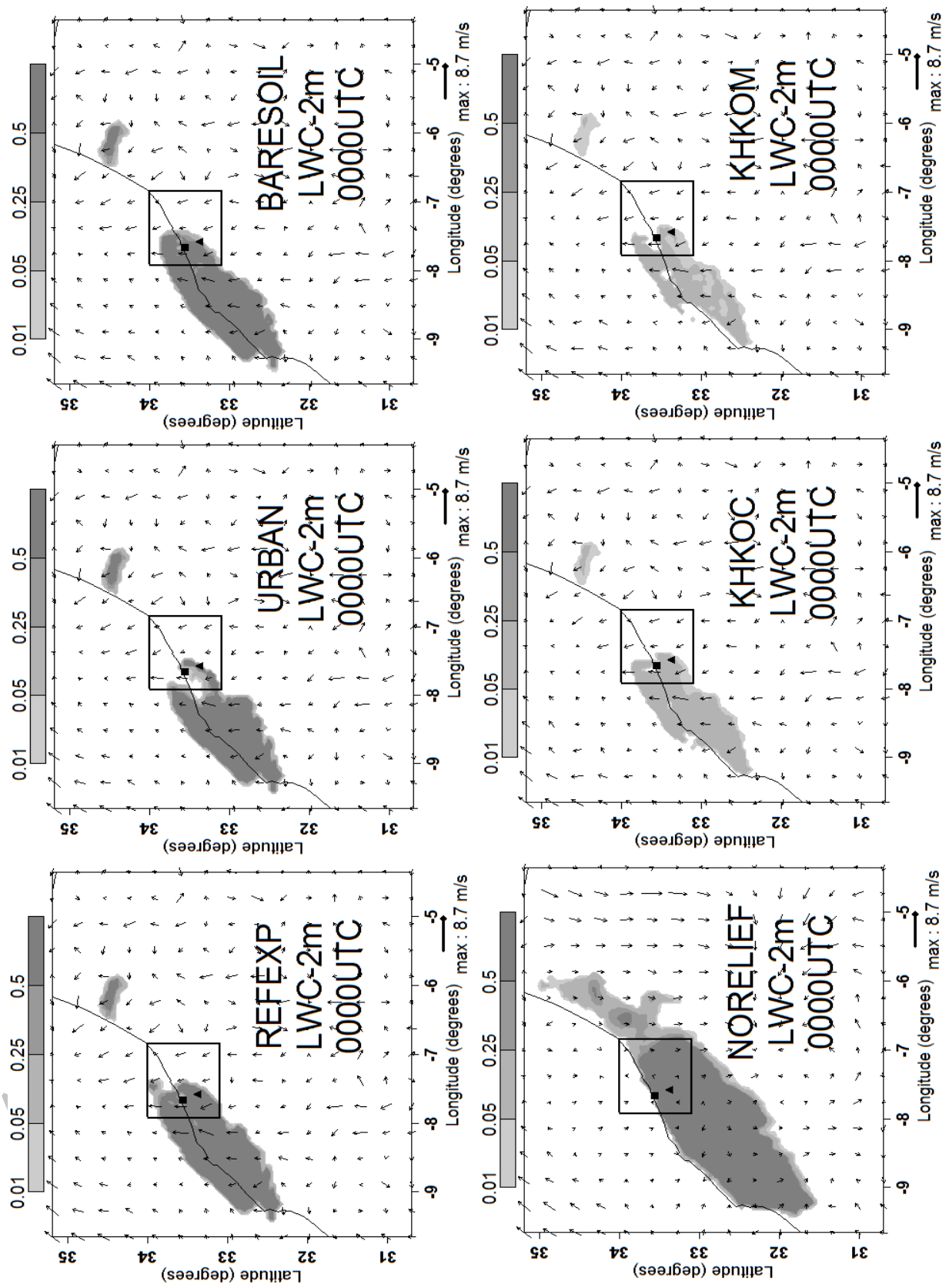

669

670 **Fig. 11.**